

Article

Role of small leucine zipper protein in hepatic gluconeogenesis and metabolic disorder

Minsoo Kang, Sun Kyoung Han, Suhyun Kim, Sungyeon Park, Yerin Jo, Hyeryung Kang, and Jesang Ko  *

Division of Life Sciences, Korea University, Seoul 02841, South Korea
*Correspondence to: Jesang Ko, E-mail: jesangko@korea.ac.kr

Edited by Feng Liu

Hepatic gluconeogenesis is the central pathway for glucose generation in the body. The imbalance between glucose synthesis and uptake leads to metabolic diseases such as obesity, diabetes, and cardiovascular diseases. Small leucine zipper protein (sLZIP) is an isoform of LZIP and it mainly functions as a transcription factor. Although sLZIP is known to regulate the transcription of genes involved in various cellular processes, the role of sLZIP in hepatic glucose metabolism is not known. In this study, we investigated the regulatory role of sLZIP in hepatic gluconeogenesis and its involvement in metabolic disorder. We found that sLZIP expression was elevated during glucose starvation, leading to the promotion of phosphoenolpyruvate carboxylase and glucose-6-phosphatase expression in hepatocytes. However, sLZIP knockdown suppressed the expression of the gluconeogenic enzymes under low glucose conditions. sLZIP also enhanced glucose production in the human liver cells and mouse primary hepatic cells. Fasting-induced cyclic adenosine monophosphate impeded sLZIP degradation. Results of glucose and pyruvate tolerance tests showed that sLZIP transgenic mice exhibited abnormal blood glucose metabolism. These findings suggest that sLZIP is a novel regulator of gluconeogenic enzyme expression and plays a role in blood glucose homeostasis during starvation.

Keywords: gluconeogenic enzymes, hepatic gluconeogenesis, hyperglycemia, transcription factor

Introduction

Blood glucose level is tightly regulated by various hormones such as insulin, glucagon, and glucocorticoids (Exton, 1979; Kraus-Friedmann, 1984; Roder et al., 2016). The liver is one of the key organs responsible for maintaining blood glucose levels; under fasting conditions, it synthesizes glucose through gluconeogenesis and releases glucose to restore a sufficient blood glucose concentration (Kraus-Friedmann, 1984). There are two key enzymes that control the rate of gluconeogenesis: phosphoenolpyruvate carboxylase (PEPCK) and glucose-6-phosphatase (G6Pase) (Lin and Accili, 2011). PEPCK converts oxaloacetate derived from pyruvate to phosphoenolpyruvate in the initial step of gluconeogenesis, and G6Pase dephosphorylates glucose-6-phosphate to produce glucose in the final step

(Rines et al., 2016). Recent studies indicate that these gluconeogenic enzymes are closely related to type II diabetic hyperglycemia and could be potential therapeutic targets for the treatment of diabetes (Rines et al., 2016). PEPCK-transgenic mice show insulin resistance and diabetes with hyperglycemia, whereas PEPCK-null mice exhibit low glucose production in a 24-h starvation state (Valera et al., 1994; Gomez-Valades et al., 2008). Furthermore, liver-specific PEPCK silencing in *db/db* mice improves glycemia and insulin sensitivity despite lipid accumulation in the liver (Gomez-Valades et al., 2008). In addition, hepatic PEPCK expression affects cataplerosis of tricarboxylic acid (TCA) cycle components (Hakimi et al., 2005; Burgess et al., 2007). G6Pase knockdown in the mouse liver increases the expression of energy expenditure-associated genes in the peripheral tissues and also protects from obesity and diabetes when a high-fat/sucrose diet is consumed (Abdul-Wahed et al., 2014). Therefore, it is important to understand the regulatory mechanism of gluconeogenic enzyme expression in metabolic diseases.

Human small leucine zipper protein (sLZIP), an isoform of LZIP (also known as CREB3), plays important roles in the expression of genes involved in proliferation, migration, and

Received May 21, 2020. Revised September 3, 2020. Accepted September 24, 2020.

© The Author(s) (2020). Published by Oxford University Press on behalf of *Journal of Molecular Cell Biology*, IBCB, SIBS, CAS.

This is an Open Access article distributed under the terms of the Creative Commons Attribution Non-Commercial License (<http://creativecommons.org/licenses/by-nc/4.0/>), which permits non-commercial re-use, distribution, and reproduction in any medium, provided the original work is properly cited. For commercial re-use, please contact journals.permissions@oup.com

differentiation in various cell types (Kang et al., 2009; Kim and Ko, 2014b; Kim et al., 2015). sLZIP negatively regulates peroxisome proliferator-activated receptor γ 2 transcriptional activation, leading to osteoblast differentiation of mesenchymal stem cells (Kim and Ko, 2014b). It also inhibits androgen receptor transcriptional activation in prostate cancer cells (Kim et al., 2015). Under Golgi stress conditions, LZIP undergoes proteolytic cleavage and the N-terminal LZIP is translocated to the nucleus, where it induces the expression of genes involved in lipid synthesis and transport in the liver (Kang et al., 2017). In addition, the N-terminal LZIP interacts with CREBH and this complex functions as a transcription factor in hepatic cells (Kang et al., 2017). CREBH enhances the transcription of PEPCK and G6Pase by binding to their promoters (Lee et al., 2010). However, the role of sLZIP in hepatic glucose metabolism remains obscure. In this study, we investigated the role of sLZIP in the regulation of gluconeogenic enzyme expression and its involvement in hepatic gluconeogenesis.

Results

sLZIP induces expression of PEPCK and G6Pase

During fasting, glucose generation is activated in order to overcome glucose-deficient environment in the liver. To examine whether glucose concentration affects sLZIP expression, we exposed HepG2 cells to low glucose conditions. The sLZIP mRNA level increased by 5.3-fold in low glucose medium in HepG2 cells (Figure 1A). Glucose deprivation induced sLZIP mRNA expression in a time-dependent manner as did PCK1 and G6PC mRNA expression in HepG2 and Huh-7 cells (Figure 1B; Supplementary Figure S1A). However, sLZIP knockdown using siRNA for sLZIP (si-sLZIP) suppressed the glucose deprivation-induced PCK1 and G6PC mRNA expression (Figure 1C; Supplementary Figure S1B). We also examined PCK1 and G6PC expression by sLZIP at both transcriptional and translational levels. Results of the luciferase reporter assay showed that sLZIP increased PEPCK and G6Pase luciferase reporter activities in a dose-dependent manner (Figure 1D). sLZIP increased both PCK1 and G6PC mRNA expression levels, whereas sLZIP knockdown dose-dependently decreased their mRNA expression (Figure 1E; Supplementary Figure S1C). sLZIP increased the protein expression level of PEPCK, whereas si-sLZIP decreased PEPCK protein expression in a dose-dependent manner (Figure 1F; Supplementary Figure S1D). These results indicate that sLZIP positively regulates the expression of PEPCK and G6Pase.

sLZIP binds to the PEPCK promoter and induces the transcriptional activation of PEPCK

sLZIP functions as a transcriptional factor and is known to bind to the CRE and AP-1 binding sites in the target gene promoters (Kim and Ko, 2014a; Kim et al., 2015). We performed luciferase activity assay using the rat PEPCK promoter to understand the regulation of PEPCK expression by sLZIP. To

determine the binding element of sLZIP in the PEPCK promoter, we generated PEPCK promoters of multiple lengths. Promoter activity was not affected until the segments were longer than the -2028 bp region of the PEPCK promoter (Figure 2A). However, the promoter activity decreased ~ 5 -fold at -1520 bp compared with the activity at -2371 bp of the PEPCK promoter (Figure 2A). These results suggest that the sLZIP binding element exists between -2028 bp and -1520 bp of the PEPCK promoter. Since there are two predicted sLZIP binding sites, CRE and AP-1, in this promoter region, we generated CRE and AP-1 mutants of the PEPCK promoter. The activity of the CRE mutant form of the PEPCK promoter was inhibited compared with that of the wild-type (WT) promoter (Figure 2B). However, the activity of the AP-1 mutant was not affected (Figure 2B). We also performed electrophoresis mobility shift assay (EMSA) using the WT and CRE mutant form of the PEPCK promoter. sLZIP interacted with the WT CRE but not with the CRE mutant, and the DNA binding affinity of sLZIP to the PEPCK promoter increased in a dose-dependent manner (Figure 2C). Results of competition experiments using a 50-fold molar excess of unlabeled probe showed that the sLZIP binding complex competed with the unlabeled sLZIP binding probe (Figure 2C), indicating that sLZIP specifically binds to the CRE site of the PEPCK promoter. We further analyzed the human PEPCK and G6Pase promoters using chromatin immunoprecipitation (ChIP) assay. Among the seven putative sLZIP binding sites in the human PEPCK promoter, sLZIP bound to CRE ($-1556/-1547$), CREBH ($-443/-437$), and CRE ($+264/+271$) in the human PEPCK promoter (Figure 2D). In addition, sLZIP bound to CRE ($-166/-160$) and CRE ($-132/-125$) in the G6Pase promoter (Figure 2E). These results indicate that sLZIP binds directly to the PEPCK promoter and regulates the transcription of PEPCK.

cAMP impedes sLZIP degradation by inhibiting ubiquitination

Cyclic adenosine monophosphate (cAMP) promotes glucose synthesis through induction of protein kinase A (PKA)-mediated gluconeogenic enzymes during fasting (Altarejos and Montminy, 2011; Han et al., 2016). We investigated the role of sLZIP as a PEPCK regulator upon cAMP stimulation under low glucose conditions. sLZIP increased PEPCK expression in the absence of 8-bromoadenosine-3',5'-cAMP (8-Br-cAMP) and also increased 8-Br-cAMP-induced PEPCK expression (Figure 3A). sLZIP knockdown decreased PEPCK expression in the absence and presence of 8-Br-cAMP (Figure 3B). 8-Br-cAMP also increased sLZIP protein expression in a dose-dependent manner, whereas it did not affect sLZIP mRNA expression (Figure 3C). To understand how cAMP increases sLZIP protein expression, we examined the protein stability of sLZIP using cycloheximide (CHX). The sLZIP protein level was maintained for a longer period of time by 8-Br-cAMP treatment (Figure 3D). Furthermore, treatment with the specific PKA inhibitor, H-89, completely abolished 8-Br-cAMP-mediated sLZIP stabilization within 6 h (Figure 3E and F). Glucagon, which activates the cAMP/PKA

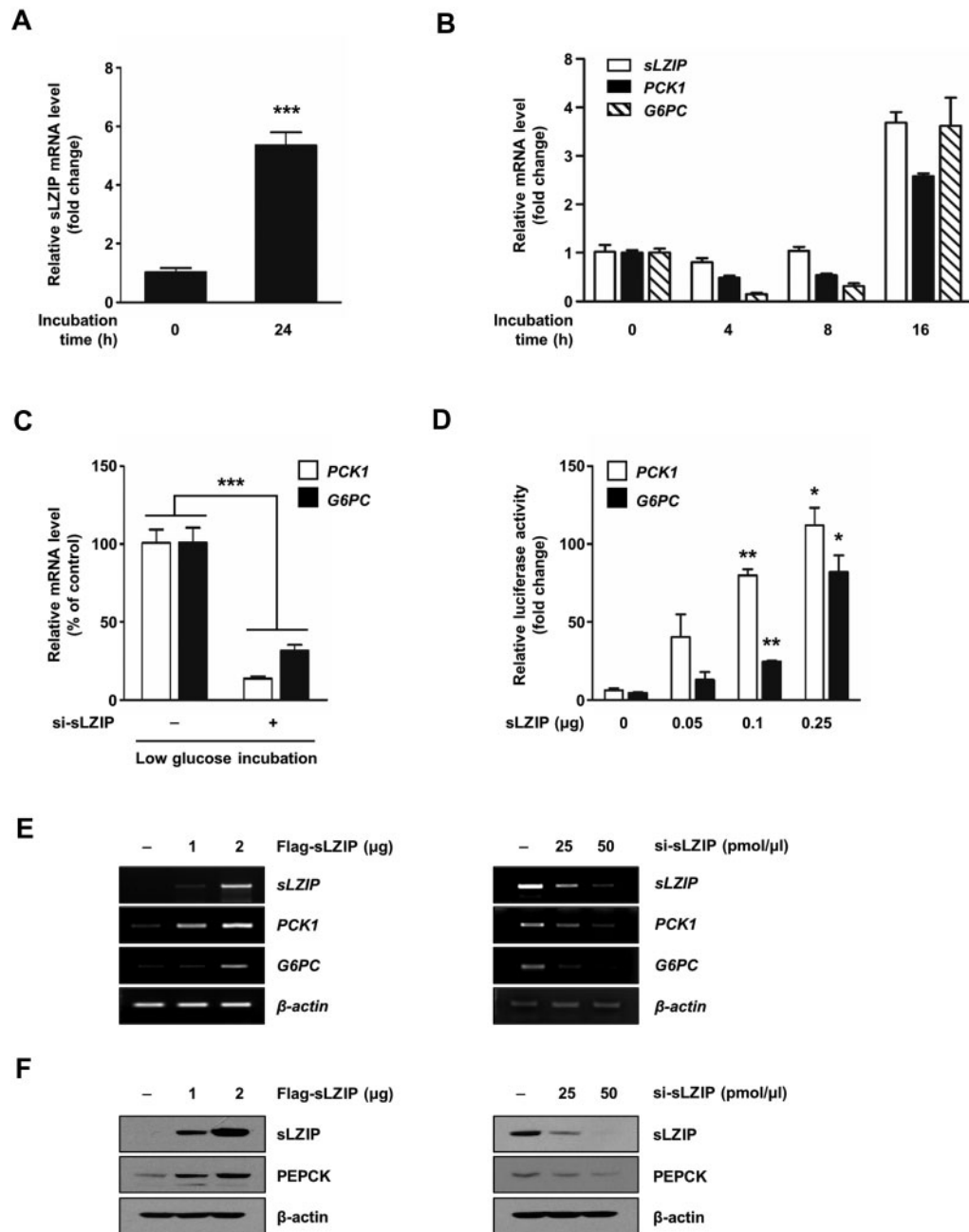


Figure 1 sLZIP induces expression of PEPCK and G6Pase. (**A** and **B**) HepG2 cells were incubated in low glucose DMEM (5 mM) for the indicated time. mRNA levels were determined by quantitative real-time polymerase chain reaction (qRT-PCR). (**C**) After siRNA (100 μ M) transfection, HepG2 cells were cultured in low glucose DMEM for 24 h. mRNA levels were determined by quantitative real-time polymerase chain reaction (qRT-PCR). (**D**) HepG2 cells were co-transfected with the indicated concentrations of sLZIP, *Renilla*-encoded vector (50 ng), and rat PEPCK promoter (0.5 μ g) or human G6PC promoter (0.5 μ g). Luciferase activities were measured after 24 h of transfection. (**E** and **F**) HepG2 cells were transfected with or without the indicated concentrations of Flag-sLZIP and si-sLZIP. (**E**) mRNA levels were determined by semi-qPCR. (**F**) Protein levels were determined by western blotting. All *P*-values were obtained using unpaired two-tailed Student's *t*-test. **P* < 0.05, ***P* < 0.01, ****P* < 0.001.

signaling, also stabilized sLZIP; however, H-89 reduced sLZIP stabilization (Figure 3E). These results indicate that cAMP is involved in sLZIP stabilization against the ubiquitin–proteasome degradation. We also examined the effect of sLZIP on

gluconeogenic gene expression induced by insulin and forskolin. Forskolin, a cytosolic cAMP inducer, induced *PCK1* and *G6PC* expression; however, sLZIP knockdown led to ~2-fold decrease in *PCK1* and *G6PC* expression (Figure 3G). Insulin

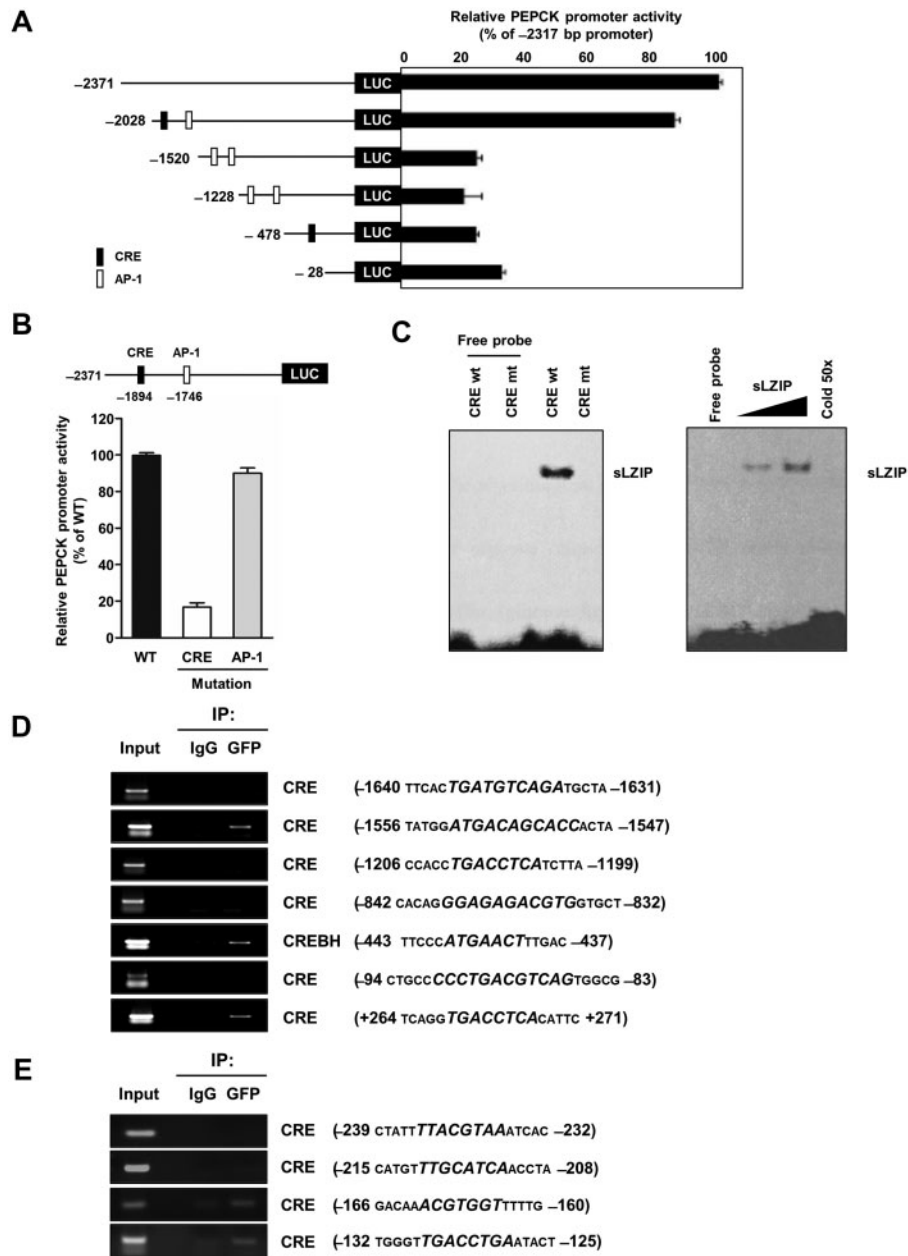


Figure 2 sLZIP binds to the PEPCK promoter and induces the transcriptional activation of PEPCK. **(A)** HepG2 cells were transfected with the truncated rat PEPCK promoters (0.5 μ g), *Renilla*-encoded vector (50 ng), and Flag-sLZIP (0.25 μ g). Luciferase activities were measured after 24 h of transfection. **(B)** HepG2 cells were transfected with the rat PEPCK promoter mutants (0.5 μ g), *Renilla*-encoded vector (50 ng), and Flag-sLZIP (0.25 μ g). Luciferase activities were measured after 24 h of transfection. **(C)** EMSA was performed using His-sLZIP (3 μ g) and the 32 P-labeled rat PEPCK-CRE probe or mutant. Each reaction mixture was loaded into the non-denaturing polyacrylamide gel and the probe-protein complex was quantified by an autoradiography film. **(D and E)** HepG2 cells were transfected with GFP-sLZIP. Immunoprecipitation was performed using 25 μ g chromatin and 5 μ g specific antibodies. ChIP samples were amplified by semi-qPCR using indicated target-specific primers.

suppressed *PCK1* and *G6PC* expression; however, sLZIP increased insulin-mediated inhibition of gluconeogenic gene expression by 2.3-fold (Figure 3H). These results indicate that cAMP promotes the transcriptional activity of sLZIP by inhibiting its protein degradation.

sLZIP promotes glucose production via PEPCK and G6Pase induction in hepatocytes

Since PEPCK and G6Pase are key enzymes for glucose production (Lin and Accili, 2011; Rines et al., 2016), we examined the effect of sLZIP on glucose production through PEPCK and

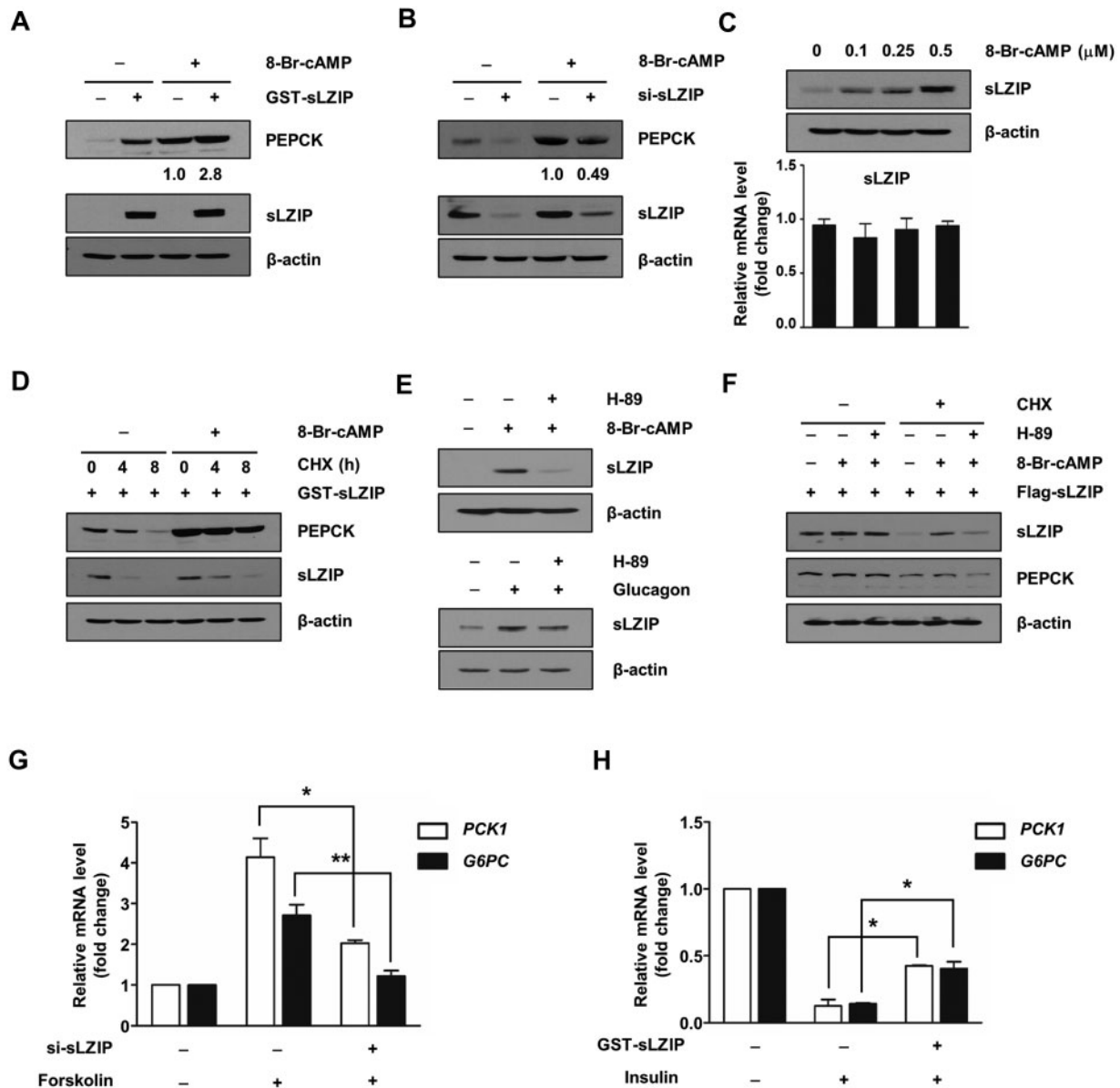


Figure 3 cAMP impedes sLZIP degradation by inhibiting ubiquitination. (**A** and **B**) HepG2 cells were transfected with GST-sLZIP (1 μg) or si-sLZIP (50 μM). After transfection, cells were incubated with 8-Br-cAMP (100 nM) in low glucose medium for 24 h. Protein levels were determined by western blotting. (**C**) HepG2 cells were treated with the indicated concentrations of 8-Br-cAMP for 24 h. Protein levels were determined by western blotting and mRNA levels were determined by qRT-PCR. (**D**) HepG2 cells were transfected with GST-sLZIP (1 μg). After transfection, cells were co-treated with 8-Br-cAMP (100 nM) and CHX (50 μM) for the indicated time. Protein levels were determined by western blotting. (**E**) Upper: HepG2 cells were co-treated with 8-Br-cAMP (125 nM) and H-89 (10 μM) for 24 h. Lower: HepG2 cells were incubated in serum-free DMEM for 18 h and pretreated with H-89 for 2 h. Then the cells were co-treated with glucagon (100 nM) and H-89 (10 μM) for 6 h in serum-free DMEM. Protein levels were determined by western blotting. (**F**) After transfection of Flag-sLZIP (1 μg), HepG2 cells were pre-treated with 8-Br-cAMP (125 nM) and H-89 (10 μM) for 2 h and treated with CHX (50 μM) for 4 h. Protein levels were determined by western blotting. (**G** and **H**) HepG2 cells were transfected with si-sLZIP (50 μM) or GST-sLZIP (1.5 μg) before treatment with forskolin (250 nM) or insulin (100 nM) for 18 h. mRNA levels were determined by qRT-PCR. All *P*-values were obtained using unpaired two-tailed Student's *t*-tests. **P* < 0.05, ***P* < 0.01.

G6Pase expression. We performed a glucose production assay to determine the glucose production ability in hepatocytes. sLZIP increased glucose secretion in a dose-dependent manner in HepG2 cells (Figure 4A). However, sLZIP knockdown dose-

dependently decreased glucose production (Figure 4B). We further investigated the role of sLZIP in hepatic gluconeogenesis using mouse primary hepatocytes. Adenoviral infection of sLZIP increased mouse *Pck1* and *G6pc* expression at the

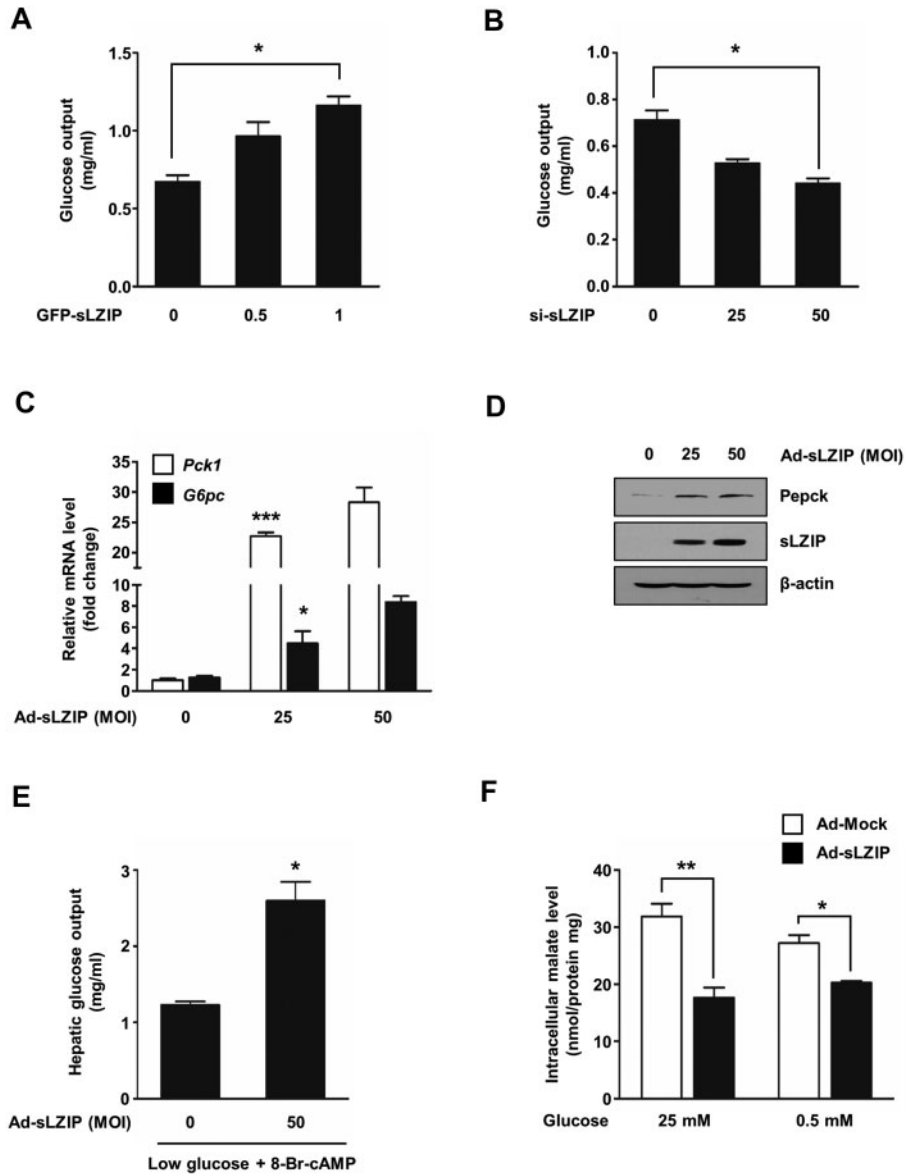


Figure 4 sLZIP promotes glucose production via PEPCK and G6Pase induction in hepatocytes. (**A** and **B**) HepG2 cells were transfected with GFP-sLZIP (1 μg) or si-sLZIP (50 μM). The glucose level was measured by ELISA using conditioned media. (**C**) Mouse primary hepatocytes were infected with Ad-sLZIP at the indicated concentrations. mRNA levels were determined by qRT-PCR. (**D**) Whole-cell lysates were obtained from Ad-sLZIP-infected mouse primary hepatocytes. Protein levels were determined by western blotting. (**E**) After Ad-sLZIP infection, mouse primary hepatocytes were incubated in low glucose medium containing 8-Br-cAMP (100 nM). The glucose level was determined by ELISA using conditioned media. (**F**) Mouse primary hepatocytes were transduced with or without Ad-sLZIP and incubated with the indicated concentrations of glucose for 3 h. The intracellular malate level was measured by ELISA. All *P*-values were obtained using unpaired two-tailed Student's *t*-tests. **P* < 0.05, ***P* < 0.01, ****P* < 0.001.

transcriptional level in a dose-dependent manner in mouse primary hepatocytes (Figure 4C). sLZIP also dose-dependently increased the PEPCK protein level (Figure 4D). In addition, sLZIP enhanced glucose secretion under fasting conditions (Figure 4E). Ectopically regulated PEPCK expression affects the distribution of TCA cycle components (Burgess et al., 2004;

Hakimi et al., 2005; Liu et al., 2018). Results of the malate assay showed that PEPCK induced by sLZIP decreased the intracellular malate level to accelerate oxaloacetate generation (Figure 4F). These results indicate that sLZIP promotes glucose production via PEPCK and G6Pase induction in both human and mouse hepatocytes.

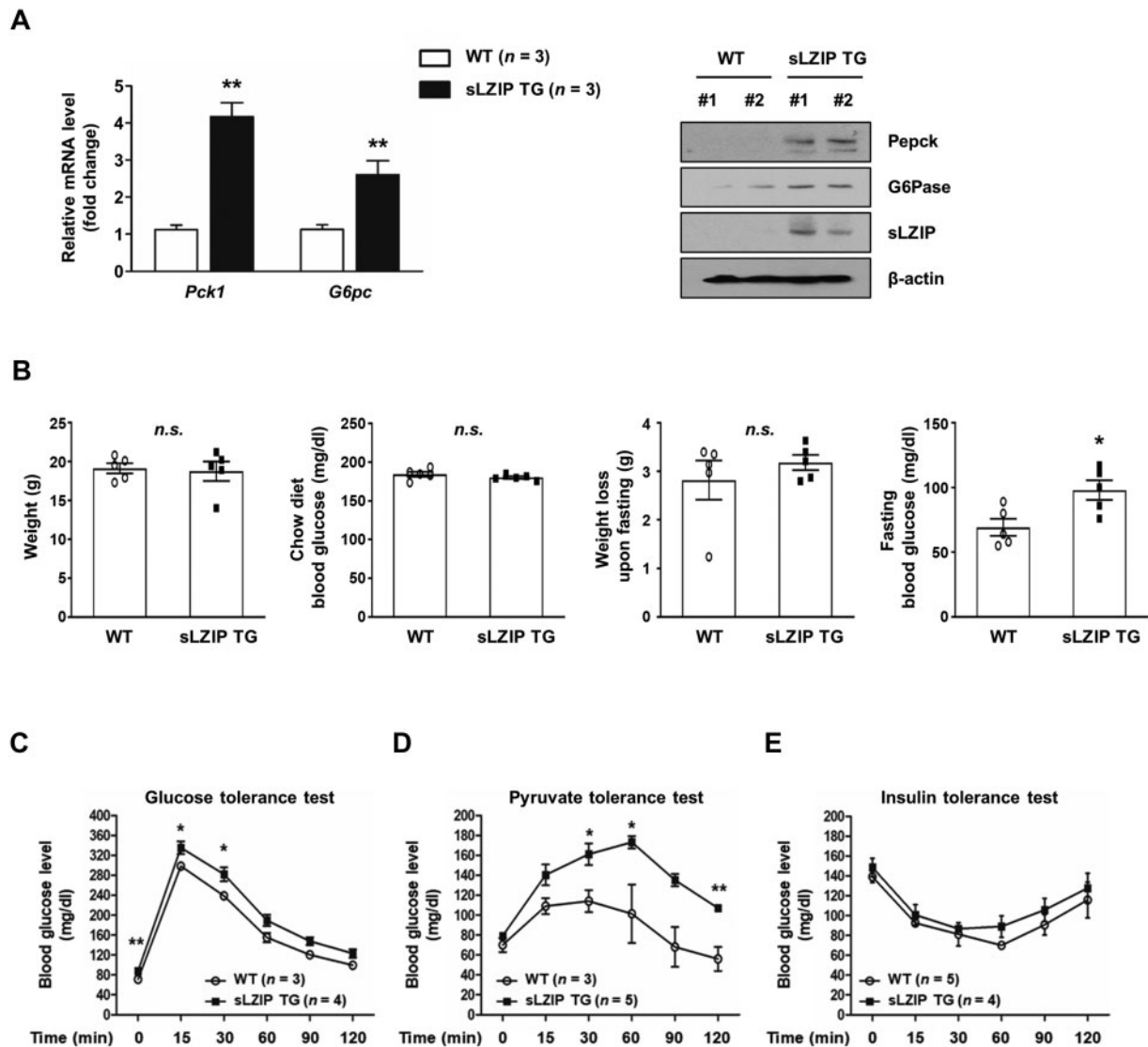


Figure 5 sLZIP TG mice show enhanced gluconeogenesis upon fasting with a normal diet. **(A)** The livers isolated from sLZIP TG and WT mice were homogenized for mRNA and protein analyses. mRNA levels were determined by qRT-PCR and protein levels were determined by western blotting. **(B)** The weight and blood glucose level were monitored in 5-week-old sLZIP TG and WT mice. After 18 h of fasting, the blood was collected from the lateral tail veins and glucose levels were measured. n.s., not significant. **(C and D)** Five-week-old sLZIP TG and WT mice were fasted for 18 h. After fasting, glucose (2 g/kg body weight, **C**) or sodium pyruvate (2 g/kg body weight, **D**) was administered by intraperitoneal injection. The blood was collected from lateral tail veins at the indicated time points. **(E)** Five-week-old sLZIP TG and WT mice were fasted for 4 h. After fasting, insulin (0.75 U/kg body weight) was administered by an intraperitoneal injection. The blood was collected from lateral tail veins at the indicated time points. All *P*-values were obtained using unpaired two-tailed Student's *t*-tests. **P* < 0.05, ***P* < 0.01.

sLZIP-transgenic mice show enhanced gluconeogenesis upon fasting with a normal diet

Since sLZIP regulates glucose production in liver cells, it is important to verify the role of sLZIP in blood glucose homeostasis *in vivo*. Therefore, we generated sLZIP-transgenic (TG) mice from the C57BL/6 strain to investigate the role of sLZIP in blood glucose homeostasis (Supplementary Figure S2A). Moreover, we determined the *Pck1* and *G6pc* mRNA levels using livers isolated from WT and sLZIP TG mice. The mRNA levels of *Pck1* and

G6pc were elevated by 4.1-fold and 2.7-fold, respectively, in the sLZIP TG mouse liver compared with the WT mouse liver (Figure 5A). Furthermore, TG mice showed increased PEPCK and G6Pase protein expression compared with WT mice (Figure 5A). However, there were no significant differences between WT and sLZIP TG mice with respect to body weight, weight loss upon fasting, and blood glucose level caused by a normal chow diet (Figure 5B). Interestingly, blood glucose levels were higher in sLZIP TG mice than in WT mice during 18 h of fasting

(Figure 5B). We next performed glucose tolerance test (GTT), pyruvate tolerance test (PTT), and insulin tolerance test (ITT) to examine the effect of sLZIP on glucose homeostasis. Results of GTT showed that sLZIP TG mice exhibited abnormal blood glucose clearance compared with the WT mice (Figure 5C). PTT results demonstrated that sLZIP TG mice showed enhanced glucose production compared with WT mice (Figure 5D). However, there was no significant difference between sLZIP TG and WT mice in insulin tolerance (Figure 5E). In addition, insulin activities were not affected by sLZIP expression in mouse adipocytes, primary hepatocytes, or HepG2 cells, indicating that sLZIP does not affect insulin-induced glucose clearance capacity (Figure 5E; Supplementary Figure S2B–E). These results indicate that sLZIP TG mice enhance hepatic gluconeogenesis upon fasting with a normal diet.

sLZIP TG mice maintain a high blood glucose level by promoting hepatic gluconeogenesis during a long-term high-fat diet

Since sLZIP promoted hepatic glucose production, we performed a long-term high-fat diet (HFD) experiment to examine the effect of sLZIP on diabetes progression. When we examined the fasting-induced fatty acid accumulation in the liver, we observed higher accumulation of lipid droplets in sLZIP TG mouse livers than the WT mouse livers during 24 h of fasting (Figure 6A). Therefore, we examined the effect of sLZIP on liver steatosis after 18 weeks of HFD. sLZIP TG mice showed slightly progressed liver steatosis compared with WT mice (Supplementary Figure S3A). During HFD, both body weight and food intake were not significantly different between sLZIP TG and WT mice (Figure 6B; Supplementary Figure S3B). There were no significant differences between WT and sLZIP TG mice in weight loss upon fasting and blood glucose level (Figure 6B). However, the blood glucose level was higher in sLZIP TG mice than in WT mice after fasting (Figure 6B). Results of GTT and PTT showed that the sLZIP TG mice exhibited abnormal glucose clearance and enhanced hepatic gluconeogenesis compared with the WT mice (Figure 6C and D). However, insulin sensitivity was not different between sLZIP TG and WT mice (Figure 6E). These results indicate that sLZIP TG mice maintain a high blood glucose level by promoting hepatic gluconeogenesis during a long-term HFD.

Discussion

Gluconeogenesis is one of the anabolic pathways that replenish low blood glucose levels (Soty et al., 2017). Although the kidney and small intestine are partially involved, hepatic gluconeogenesis accounts for a great part of the glucose production (Soty et al., 2017). Therefore, understanding the molecular mechanism of gluconeogenesis in the liver is important for controlling glucose metabolism. In this study, we found that sLZIP expression was increased in hepatic cells under low

glucose conditions and promoted both PEPCK and G6Pase expression. Moreover, sLZIP promoted glucose secretion in human and mouse hepatocytes in a dose-dependent manner. We also found that fasting significantly increased the accumulation of lipid droplets in sLZIP TG mice compared with WT mice. These results indicate that sLZIP TG mice obtain carbon sources more efficiently for glucose generation compared with WT mice. Our previous study suggested that activation of LZIP is required for APOA4 expression and contributes to free fatty acid uptake in the liver (Kang et al., 2017). Although further studies are needed to characterize the effects of two LZIP isoforms, our results suggest that sLZIP can be a novel regulator for controlling glucose production in the liver.

We found that sLZIP directly bound to several CRE regions in the PEPCK promoter and induced PEPCK transcription. sLZIP also recognized the CREBH binding element. Several studies indicate that members of the CREB3 family can interact with each other (Reinke et al., 2013; Chen et al., 2014; Huttlin et al., 2017). The N-terminal region of LZIP interacts with CREBH and they share the binding element in the APOA4 promoter (Kang et al., 2017). Since the function of CREBH is well established in hepatic gluconeogenesis and liver steatosis (Lee et al., 2010; Zhang et al., 2012), it is possible that the sLZIP/CREBH complex regulates PEPCK and G6Pase expression. Co-expression of sLZIP and CREBH increased *PCK1* promoter activity compared with the expression of sLZIP or CREBH alone (Supplementary Figure S4A). In addition, sLZIP bound to the N-terminal of CREBH in HepG2 cells (Supplementary Figure S4B). Co-expression of sLZIP and CREBH synergistically increased PEPCK expression at both transcriptional and translational levels (Supplementary Figure S4C and D). Although further studies are required for understanding the exact mechanism of glucose production by the sLZIP/CREBH complex, these findings support that sLZIP plays important roles in glucose and lipid metabolism in the liver.

The cAMP/PKA signaling induces PEPCK expression (Altarejos and Montminy, 2011; Han et al., 2016). We found that sLZIP increased PEPCK expression in the absence or presence of 8-Br-cAMP. Since sLZIP-induced PEPCK expression was enhanced by the presence of 8-Br-cAMP, we investigated the effect of cAMP on sLZIP regulation. The cAMP/PKA signaling is closely associated with the ubiquitin–proteasome pathway (Huang et al., 2013). It has been reported that elevated cAMP reduces proteasome activity and inhibits the expression of E3 ubiquitin ligases (Goncalves et al., 2009; Lira et al., 2011). Therefore, we examined whether the cAMP/PKA signaling was involved in sLZIP stabilization against the ubiquitin–proteasome degradation. We found that cAMP blocked sLZIP degradation by inhibiting ubiquitination.

Recent studies have reported a process called cataplerosis, by which PEPCK contributes to cancer progression by removing TCA cycle intermediates regardless of gluconeogenesis (Leithner et al., 2015; Li et al., 2015; Montal et al., 2015; Vincent et al., 2015). Elevated PEPCK improves glucose and glutamine utilization to promote lipogenesis and the pentose

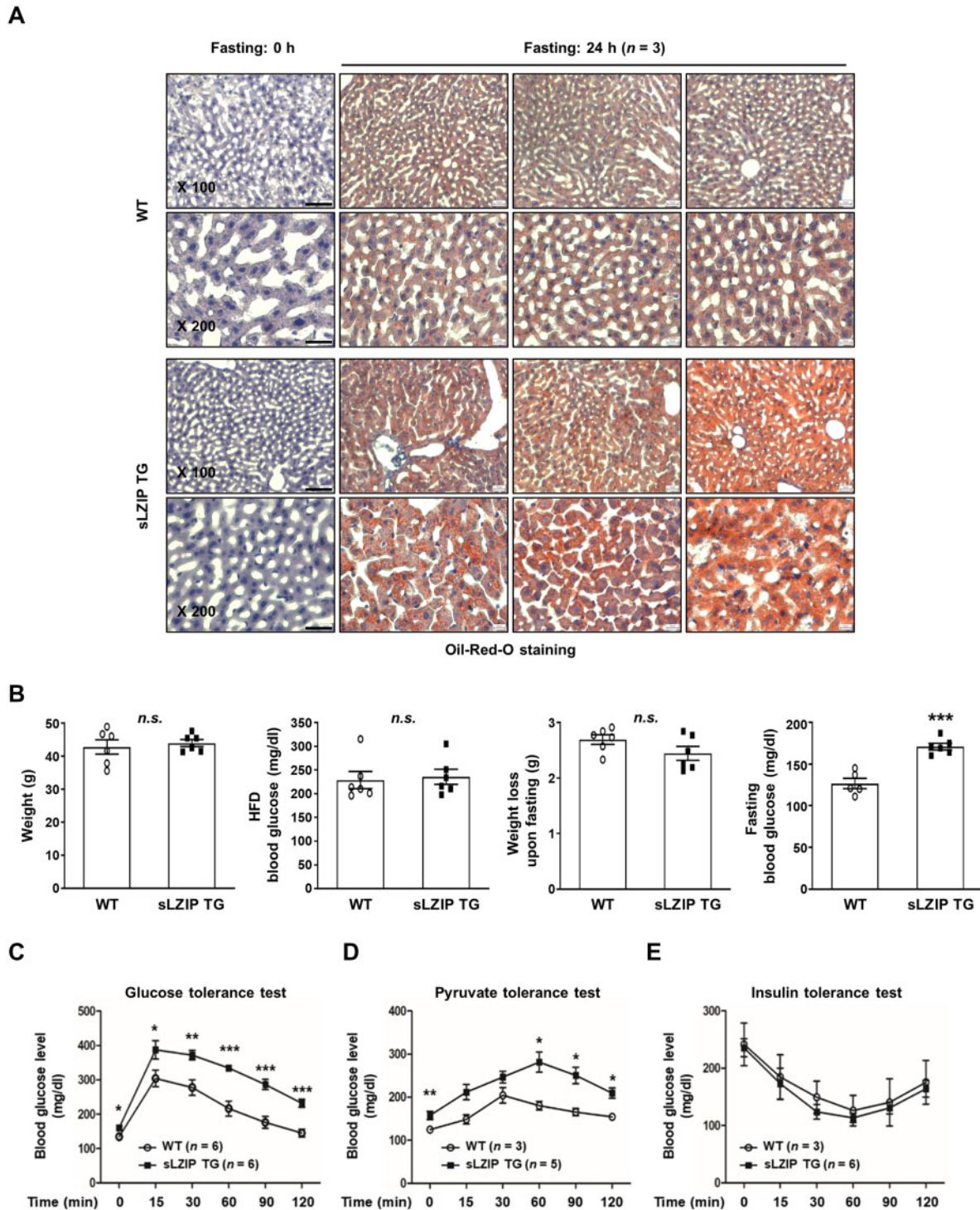


Figure 6 sLZIP TG mice maintain a high blood glucose level by promoting hepatic gluconeogenesis during a long-term HFD. **(A)** Frozen liver tissues were stained with Oil-Red-O and hematoxylin. Red dots: lipid droplets; blue: nucleus. Scale bar, 100 μ m. **(B)** After HFD, sLZIP TG and WT mice were subjected to observation of weight and blood glucose levels. The blood was collected from the lateral tail veins and glucose levels were measured after fasting for 18 h. n.s., not significant. **(C and D)** sLZIP TG and WT mice fed with HFD were fasted for 18 h. After fasting, glucose (1 g/kg body weight, **C**) or sodium pyruvate (1 g/kg body weight, **D**) was administrated by intraperitoneal injection. Blood was collected from lateral tail veins at the indicated time points. **(E)** sLZIP TG and WT mice fed with HFD were fasted for 4 h. After fasting, insulin (1.5 U/kg body weight) was administrated by intraperitoneal injection. Blood was collected from the lateral tail veins at the indicated time points. All *P*-values were obtained using unpaired two-tailed Student's *t*-tests. **P* < 0.05, ***P* < 0.01, ****P* < 0.001.

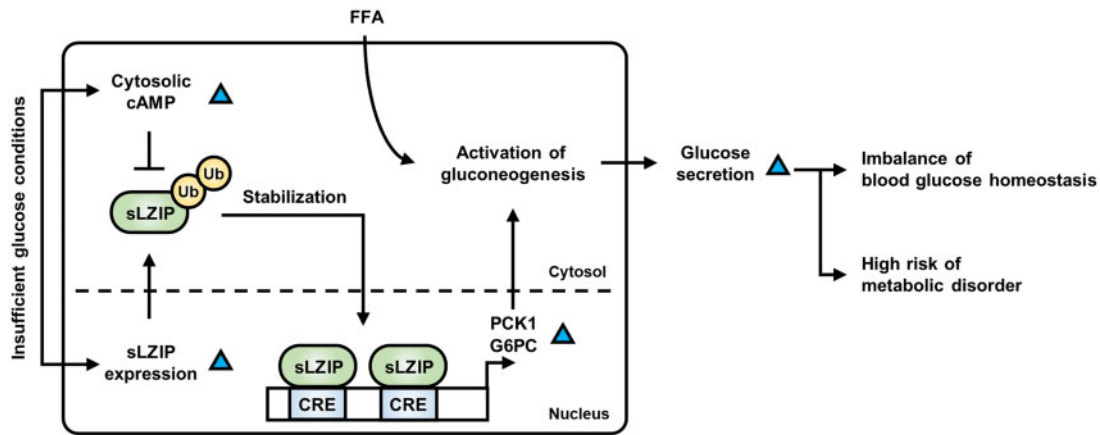


Figure 7 Schematic diagram of the regulatory mechanism of gluconeogenesis by sLZIP.

phosphate pathway, which induce colon cancer cell proliferation (Montal et al., 2015). In melanoma tumor-repopulating cells, PEPCK is involved in glucose consumption and *in vivo* tumorigenesis (Li et al., 2015). Moreover, mitochondrial PEPCK not only provides resistance to glucose depletion but also contributes to phosphoenolpyruvate accumulation to adapt to low glucose conditions in non-small cell lung cancer (Leithner et al., 2015; Vincent et al., 2015). Thus, many cancer cells benefit from elevated levels of gluconeogenesis intermediates. sLZIP acts as a regulator in various cancers, including prostate, breast, and cervical cancers (Kang et al., 2011; Kim et al., 2015; Jeong et al., 2017). Since elevated sLZIP reduced the intracellular malate levels in both high and low glucose conditions, sLZIP may play a role in cancer metabolism by inducing PEPCK expression.

Insulin signaling, which is usually activated by increased blood glucose levels, is crucial for gluconeogenesis suppression in the liver and glucose consumption in other peripheral tissues. Compared to WT mice, sLZIP TG mice showed enhanced gluconeogenesis when external pyruvate was supplied. They also showed reduced glucose clearance ability compared with WT mice. However, insulin sensitivity was not significantly different between the TG and WT mice. In a previous study, TFE3 (a member of HLH-leucine zipper transcription factors) knockdown mice exhibited glucose intolerance by secretion of insufficient insulin, but no significant difference was observed in ITT (Pastore et al., 2017). PLPP1-depletion mice show diminished hepatic gluconeogenesis, without a change in insulin secretion and glucose tolerance (Taddeo et al., 2017). SMILE-deletion mice showed suppressed glucose clearance and increased hepatic glucose production, but insulin resistance was not affected (Lee et al., 2016). Primary hepatocytes from SMILE-depleted mice enhance glucose secretion and gluconeogenic gene expression by long insulin stimulation but not by short insulin stimulation (Lee et al., 2016). Our results showed that sLZIP sustained the expression level of *PCK1* and *G6PC* by long insulin stimulation, and insulin sensitivities were not

changed by sLZIP expression in adipocytes and hepatocytes. Thus, sLZIP might be involved in the insulin-independent regulation of hepatic gluconeogenesis via induction of gluconeogenic enzymes.

In diabetes mellitus, chronic hyperglycemia by abnormal glucose metabolism causes multiple complications including diabetic retinopathy, neuropathy, and nephropathy (Chawla et al., 2016). Previous studies demonstrated that glomerular hypertrophy and mesangial expansion, which are a central manifestation of diabetic nephropathy, were developed and stimulated by high glucose levels (Abrass, 1995; Wolf and Ziyadeh, 1999; Mahimainathan et al., 2006). sLZIP TG mice exhibited lower high-density lipoprotein composition in serum during HFD, which can lead to diabetes or hypertension (Supplementary Figure S3C). Furthermore, hypertension concomitant with hyperglycemia is a hallmark of diabetes that progressively damages blood vessels and glomeruli (Wolf and Ziyadeh, 1999; Chawla et al., 2016). These results suggest that sLZIP is beneficial for the progression of metabolic disorders, as it contributes to hyperglycemia.

In conclusion, sLZIP expression was induced under fasting conditions and further upregulated PEPCK and G6Pase expression, resulting in glucose production and secretion (Figure 7). sLZIP TG mice showed enhanced hepatic gluconeogenesis and decreased blood glucose clearance ability compared with WT mice. These findings suggest that sLZIP functions as a novel modulator of glucose metabolism via regulation of hepatic gluconeogenesis. Thus, sLZIP can be a potential therapeutic target for the treatment of metabolic diseases.

Materials and methods

Materials

Dulbecco's Modified Eagle's Medium (DMEM; 12800-017) was purchased from Thermo Fisher Scientific. Fetal bovine serum (FBS) was obtained from Hyclone Laboratory. Rabbit polyclonal antibody recognizing G6Pase- α (sc-25840) and mouse

monoclonal antibodies recognizing β -actin (sc-47778), GST (sc-138), and GFP (sc-9996) were purchased from Santa Cruz Biotechnology. Mouse monoclonal anti-HA antibody (G036) was purchased from Applied Biological Materials (abm). Rabbit polyclonal anti-PCK1 antibody (12940S) was obtained from Cell Signaling Technology. Mouse monoclonal anti-Flag-M2 antibody (F1804), glucagon (G2044), and 8-Br-cAMP (B5386) were purchased from Millipore Sigma. Hematoxylin Mayer's & eosin Y solution (H&E) was obtained from Labcore.

Cell culture

HepG2 and Huh-7 cells were maintained in DMEM supplemented with 10% FBS and 1% antibiotic solution. Mouse primary hepatocytes were isolated as previously described (Kang et al., 2017). Briefly, after perfusion using collagenase-HEPES buffer, hepatocytes were collected by passing through a cell strainer. Cells were mixed with Percoll (Millipore Sigma, P4937) and centrifuged at $1000\times g$ for 5 min. The hepatocytes were maintained in M199 supplemented with 23 mM HEPES, 1 nM dexamethasone, 1 nM insulin, 10% FBS, and 1% antibiotic solution. After incubation for 2 h, the medium was replaced with M199 not containing FBS.

Plasmids and mutant constructs

For transfection, human sLZIP was inserted into the pCMV-3tag-1 plasmid vector (Agilent Technologies). For the luciferase assay, plasmid vectors of rat *Pck1*-Luc (−2371 bp/+72 bp) and human *G6pc*-Luc (−1227 bp/+57 bp), gifts from Dr Hueng-Sik Choi (Chunnam National University, South Korea), were used. A series of rat PCK1 promoters were inserted into the pGL4.21 plasmid vector (Promega) using the restriction enzymes *KpnI* and *XhoI*. The primer sequences used are listed in [Supplementary Table S1A](#). For promoter mutagenesis, CRE (−1894 bp/−1887 bp) and AP-1 (−1746 bp/−1735 bp) binding sites in the rat PCK1 promoter were mutated using the QuickChange II Site-Directed Mutagenesis Kit (Agilent Technologies) according to the manufacturer's protocol. Sequences of the primers used are listed in [Supplementary Table S1B](#).

Transfection and western blotting

Cells were plated at a density of 3.5×10^5 cells/well and transfected with plasmids using E-fectin plus (Lugen Science) and incubated for 24 h. For siRNA transfection, cells were transfected with siRNA using Interferin (Polyplus-transfection) according to the manufacturer's protocol. The sequence of si-sLZIP is 5'-CCAGAUGACUCCACAGCAU-3'. Cells transfected with Mock-vector or scrambled siRNA were used as the negative control. For western blotting, cells were lysed in RIPA buffer on ice and centrifuged at $12000\times g$ for 20 min at 4°C. Equal amounts of proteins were subjected to 10% SDS-PAGE and transferred to nitrocellulose membranes. The membranes were probed with specific antibodies at 4°C overnight. β -actin was used as an internal control. The blots were then incubated with

secondary antibody at 25°C for 1 h. The immune complex was detected using WestSave Gold (Young In Frontier).

RNA isolation and qRT-PCR

Total RNA was isolated using TaKaRa MiniBEST Universal RNA Extraction Kit (Takara Bio) according to the manufacturer's protocol. cDNA was synthesized from total RNA using 5 \times PrimeScript RT master mix (Takara Bio) according to the manufacturer's protocol. Then, qRT-PCR was performed on the QuantStudio3 instrument (Thermo Fisher Scientific) using EvaGreen express 2 \times master mix (abm). Sequences of primers used for qRT-PCR are listed in [Supplementary Table S1C](#).

Luciferase activity assay

Luciferase activity assay was performed using the Dual-Luciferase Reporter Assay system (Promega, E1910). Cells were transfected with recombinant pGL4.21-*Pck1* and *G6pc* promoter plasmid vectors and the pRL-CMV Renilla plasmid vector. Renilla was used as an internal control. Cells were washed with cold phosphate-buffered saline (PBS) and lysed with cell lysis buffer. Luciferase activity was measured using a Luminometer 20/20ⁿ (Promega) according to the manufacturer's protocol.

EMSA

Probes were labeled at the 5' end with [γ -³²P]ATP using T4 polynucleotide kinase (Promega). EMSA was performed as previously described (Kim and Ko, 2014b). Briefly, His-sLZIP was pre-incubated in the 5 \times binding buffer for 10 min at 25°C. For competitor, His-sLZIP was incubated with an excess of the unlabeled probe prior to the addition of the radiolabeled probe. Each reaction mixture was then loaded into the well of a 4% nondenaturing polyacrylamide gel. The gel was dried for 1 h and exposed to an autoradiography film at −80°C. Sequences of primers used for EMSA are listed in [Supplementary Table S1D](#).

Immunoprecipitation assay

Cells were lysed with lysis buffer (25 mM Tris-HCl, pH 7.4, 150 mM NaCl, 1% NP-40, 1 mM EDTA, and 5% glycerol). Total lysates were mixed with protein A/G beads (Santa Cruz Biotechnology, sc-2003) and 5 μ g anti-IgG or anti-PCK1 antibody at 4°C for 16 h. The mixture was centrifuged at $500\times g$ for 5 min at 4°C, and the pellet was washed thrice with 1 ml cold PBS. The pellets were then mixed with the same volume of 2 \times protein loading dye and boiled at 100°C for 10 min. The supernatants were centrifuged at $12000\times g$ for 1 min and subjected to western blotting analysis as described above.

ChIP assay

Cells were treated with formaldehyde (final concentration, 0.75%; Millipore Sigma) and rotated at 25°C for 15 min. Glycine was added before scraping with cold PBS. Pellets were lysed using sonication with FA lysis buffer. Chromatin samples were co-incubated with protein A/G beads and

anti-IgG or anti-HA antibody. Samples were treated with proteinase K (5 mg/ml) at 65°C for 6 h, followed by phenol/chloroform DNA extraction. Pellets were dissolved in 30 ml distilled deionized water. The primer sequences used are listed in [Supplementary Table S1E](#).

Cell-based glucose and malate measurement

Glucose concentration was measured by the glucose assay kit (Millipore Sigma) according to the manufacturer's protocol. Briefly, conditioned medium was diluted with deionized water and mixed with o-dianosidine and 12 N H₂SO₄. Intracellular glucose levels were determined at 540 nM using a microplate reader (Bio-Rad). For the malate assay, mouse primary hepatocytes were infected with or without Ad-sLZIP. The cells were then incubated with 25 mM or 0.5 mM glucose-containing medium for 3 h. The intracellular malate concentration was determined using the malate assay kit (Biovision) using a microplate reader (Bio-Rad).

Animal study

C57BL6 mice were purchased from Orient Bio Inc. sLZIP TG mice were generated as previously described ([Kim and Ko, 2014b](#)). Briefly, the pCMV-3Tag-1 vector containing a 1062-bp coding region encoding 354 amino acids of sLZIP protein was used for generation of sLZIP TG mice. TG founders were mated with WT C57BL/6 mice to produce F1 heterozygotes. F1–F4 generations were genetically screened for the transgene at 2-week-old age. Genomic DNA was purified from mouse tail, and the *sLZIP* gene was amplified using the Phire Animal Tissue Direct PCR Kit (Thermo Fisher Scientific) according to the manufacturer's instructions. Mice were maintained at 22°C ± 2°C and 50% ± 10% humidity under 12-h light:12-h dark regimen. The Institutional Animal Care and Use Committee of Korea University approved the studies, which were performed under the guidelines for care and use of laboratory animals. For HFD, 60% kcal fat diet (Research Diets, Inc.) was fed to 5-week-old male mice up to 23 weeks.

Blood glucose measurement

For GTT, glucose (2 g/kg body weight) or PBS was intraperitoneally injected into 5- to 6-week-old male mice after 18 h of fasting. For HFD, mice were injected with glucose (1 g/kg body weight) or PBS after 18 weeks of HFD feeding and 18 h of fasting. For PTT, sodium pyruvate (2 g/kg body weight) or PBS was intraperitoneally injected into 5- to 6-week-old male mice after 18 h of fasting. For HFD, mice were injected with sodium pyruvate (1 g/kg body weight) or PBS after 18 weeks of HFD feeding and 18 h of fasting. For ITT, insulin (0.75 U/kg body weight) or PBS was intraperitoneally injected into 5 to 6-week-old male mice after 4 h of fasting. For HFD, mice were injected with insulin (1.5 U/kg body weight) or PBS after 18 weeks of HFD feeding and 4 h of fasting. Blood glucose levels were measured using the Roche Accu-Chek Active Strip.

Histological analysis

Mice were anesthetized using isoflurane and sacrificed by trans-cardiac perfusion using 4% paraformaldehyde (PFA) containing PBS. Mouse liver was isolated, incubated with 4% PFA at 4°C for 4 h, and washed twice with PBS. The fixed liver was incubated with 30% sucrose PBS buffer at 4°C for 48 h and mounted on a chuck with Tissue-Tek Optimal Cutting Temperature compound (Sakura Finetek Japan). After freezing, liver samples were sliced (10-μm thickness) using a cryotome (Leica). After air-drying, tissue slices were stained with H&E according to the manufacturer's protocols. Oil-Red-O staining was performed as previously described ([Kang et al., 2017](#)).

Statistical analysis

Data are presented as mean ± standard error of the mean. Statistical evaluation was performed using GraphPad Prism Software 5 (GraphPad Software). Two-tailed *t*-test was used to determine the differences between two means. *P*-value of 0.05 or less was considered to indicate statistical significance.

Supplementary material

[Supplementary material](#) is available at *Journal of Molecular Cell Biology* online.

Acknowledgements

The authors thank Dr Hueng-Sik Choi (Chunnam National University, South Korea) for supplying plasmid vectors of rat *Pck1*-Luc and human *G6pc*-Luc.

Funding

This research was supported by Basic Science Research Program through the National Research Foundation of Korea (NRF) funded by the Ministry of Science, ICT and Future Planning (NRF-2017R1E1A1A01073955) and the Korea University Grant.

Conflict of interest: none declared.

Author contributions: M.K. and J.K. participated in conception and design of the experiments, contributed to data analysis and interpretation, and wrote the manuscript; M.K., S.K.H., S.K., S.P., Y.J., and H.K. performed experiments.

References

- Abdul-Wahed, A., Gautier-Stein, A., Casteras, S., et al. (2014). A link between hepatic glucose production and peripheral energy metabolism via hepatokines. *Mol. Metab.* 3, 531–543.
- Abrass, C.K. (1995). Diabetic nephropathy. Mechanisms of mesangial matrix expansion. *West. J. Med.* 162, 318–321.

- Altarejos, J.Y., and Montminy, M. (2011). CREB and the CRTC co-activators: sensors for hormonal and metabolic signals. *Nat. Rev. Mol. Cell Biol.* **12**, 141–151.
- Burgess, S.C., Hausler, N., Merritt, M., et al. (2004). Impaired tricarboxylic acid cycle activity in mouse livers lacking cytosolic phosphoenolpyruvate carboxykinase. *J. Biol. Chem.* **279**, 48941–48949.
- Burgess, S.C., He, T., Yan, Z., et al. (2007). Cytosolic phosphoenolpyruvate carboxykinase does not solely control the rate of hepatic gluconeogenesis in the intact mouse liver. *Cell Metab.* **5**, 313–320.
- Chawla, A., Chawla, R., and Jaggi, S. (2016). Microvascular and macrovascular complications in diabetes mellitus: Distinct or continuum? *Indian J. Endocrinol. Metab.* **20**, 546–551.
- Chen, T.C., Lin, K.T., Chen, C.H., et al. (2014). Using an in situ proximity ligation assay to systematically profile endogenous protein–protein interactions in a pathway network. *J. Proteome Res.* **13**, 5339–5346.
- Exton, J.H. (1979). Regulation of gluconeogenesis by glucocorticoids. *Monogr. Endocrinol.* **12**, 535–546.
- Gomez-Valades, A.G., Mendez-Lucas, A., Vidal-Alabro, A., et al. (2008). Pck1 gene silencing in the liver improves glycemia control, insulin sensitivity, and dyslipidemia in db/db mice. *Diabetes* **57**, 2199–2210.
- Goncalves, D.A., Lira, E.C., Baviera, A.M., et al. (2009). Mechanisms involved in 3',5'-cyclic adenosine monophosphate-mediated inhibition of the ubiquitin–proteasome system in skeletal muscle. *Endocrinology* **150**, 5395–5404.
- Hakimi, P., Johnson, M.T., Yang, J., et al. (2005). Phosphoenolpyruvate carboxykinase and the critical role of cataplerosis in the control of hepatic metabolism. *Nutr. Metab.* **2**, 33.
- Han, H.S., Kang, G., Kim, J.S., et al. (2016). Regulation of glucose metabolism from a liver-centric perspective. *Exp. Mol. Med.* **48**, e218.
- Huang, H., Wang, H., and Figueiredo-Pereira, M.E. (2013). Regulating the ubiquitin/proteasome pathway via cAMP-signaling: neuroprotective potential. *Cell Biochem. Biophys.* **67**, 55–66.
- Huttlin, E.L., Bruckner, R.J., Paulo, J.A., et al. (2017). Architecture of the human interactome defines protein communities and disease networks. *Nature* **545**, 505–509.
- Jeong, J., Park, S., An, H.T., et al. (2017). Small leucine zipper protein functions as a negative regulator of estrogen receptor α in breast cancer. *PLoS One* **12**, e0180197.
- Kang, H., Jang, S.W., and Ko, J. (2011). Human leucine zipper protein sLZIP induces migration and invasion of cervical cancer cells via expression of matrix metalloproteinase-9. *J. Biol. Chem.* **286**, 42072–42081.
- Kang, M., Kim, J., An, H.T., et al. (2017). Human leucine zipper protein promotes hepatic steatosis via induction of apolipoprotein A-IV. *FASEB J.* **31**, 2548–2561.
- Kang, H., Kim, Y.S., and Ko, J. (2009). A novel isoform of human LZIP negatively regulates the transactivation of the glucocorticoid receptor. *Mol. Endocrinol.* **23**, 1746–1757.
- Kim, Y., Kim, J., Jang, S.W., et al. (2015). The role of sLZIP in cyclin D3-mediated negative regulation of androgen receptor transactivation and its involvement in prostate cancer. *Oncogene* **34**, 226–236.
- Kim, J., and Ko, J. (2014a). Human sLZIP promotes atherosclerosis via MMP-9 transcription and vascular smooth muscle cell migration. *FASEB J.* **28**, 5010–5021.
- Kim, J., and Ko, J. (2014b). A novel PPAR γ 2 modulator sLZIP controls the balance between adipogenesis and osteogenesis during mesenchymal stem cell differentiation. *Cell Death Differ.* **21**, 1642–1655.
- Kraus-Friedmann, N. (1984). Hormonal regulation of hepatic gluconeogenesis. *Physiol. Rev.* **64**, 170–259.
- Lee, M.W., Chanda, D., Yang, J., et al. (2010). Regulation of hepatic gluconeogenesis by an ER-bound transcription factor, CREBH. *Cell Metab.* **11**, 331–339.
- Lee, J.M., Seo, W.Y., Han, H.S., et al. (2016). Insulin-inducible SMILE inhibits hepatic gluconeogenesis. *Diabetes* **65**, 62–73.
- Leithner, K., Hrzenjak, A., Trotsmuller, M., et al. (2015). PCK2 activation mediates an adaptive response to glucose depletion in lung cancer. *Oncogene* **34**, 1044–1050.
- Li, Y., Luo, S., Ma, R., et al. (2015). Upregulation of cytosolic phosphoenolpyruvate carboxykinase is a critical metabolic event in melanoma cells that repopulate tumors. *Cancer Res.* **75**, 1191–1196.
- Lin, H.V., and Accili, D. (2011). Hormonal regulation of hepatic glucose production in health and disease. *Cell Metab.* **14**, 9–19.
- Lira, E.C., Goncalves, D.A., Parreiras, E.S.L.T., et al. (2011). Phosphodiesterase-4 inhibition reduces proteolysis and atrogenes expression in rat skeletal muscles. *Muscle Nerve* **44**, 371–381.
- Liu, M.X., Jin, L., Sun, S.J., et al. (2018). Metabolic reprogramming by PCK1 promotes TCA cataplerosis, oxidative stress and apoptosis in liver cancer cells and suppresses hepatocellular carcinoma. *Oncogene* **37**, 1637–1653.
- Mahimainathan, L., Das, F., Venkatesan, B., et al. (2006). Mesangial cell hypertrophy by high glucose is mediated by downregulation of the tumor suppressor PTEN. *Diabetes* **55**, 2115–2125.
- Montal, E.D., Dewi, R., Bhalla, K., et al. (2015). PEPCK coordinates the regulation of central carbon metabolism to promote cancer cell growth. *Mol. Cell* **60**, 571–583.
- Pastore, N., Vainshtein, A., Klisch, T.J., et al. (2017). TFE3 regulates whole-body energy metabolism in cooperation with TFEb. *EMBO Mol. Med.* **9**, 605–621.
- Reinke, A.W., Baek, J., Ashenberg, O., et al. (2013). Networks of bZIP protein–protein interactions diversified over a billion years of evolution. *Science* **340**, 730–734.
- Rines, A.K., Sharabi, K., Tavares, C.D., et al. (2016). Targeting hepatic glucose metabolism in the treatment of type 2 diabetes. *Nat. Rev. Drug Discov.* **15**, 786–804.
- Roder, P.V., Wu, B., Liu, Y., et al. (2016). Pancreatic regulation of glucose homeostasis. *Exp. Mol. Med.* **48**, e219.
- Soty, M., Gautier-Stein, A., Rajas, F., et al. (2017). Gut–brain glucose signaling in energy homeostasis. *Cell Metab.* **25**, 1231–1242.
- Taddeo, E.P., Hargett, S.R., Lahiri, S., et al. (2017). Lysophosphatidic acid counteracts glucagon-induced hepatocyte glucose production via STAT3. *Sci. Rep.* **7**, 127.
- Valera, A., Pujol, A., Pelegrin, M., et al. (1994). Transgenic mice overexpressing phosphoenolpyruvate carboxykinase develop non-insulin-dependent diabetes mellitus. *Proc. Natl Acad. Sci. USA* **91**, 9151–9154.
- Vincent, E.E., Sergushichev, A., Griss, T., et al. (2015). Mitochondrial phosphoenolpyruvate carboxykinase regulates metabolic adaptation and enables glucose-independent tumor growth. *Mol. Cell* **60**, 195–207.
- Wolf, G., and Ziyadeh, F.N. (1999). Molecular mechanisms of diabetic renal hypertrophy. *Kidney Int.* **56**, 393–405.
- Zhang, C., Wang, G., Zheng, Z., et al. (2012). Endoplasmic reticulum-tethered transcription factor cAMP responsive element-binding protein, hepatocyte specific, regulates hepatic lipogenesis, fatty acid oxidation, and lipolysis upon metabolic stress in mice. *Hepatology* **55**, 1070–1082.